Silicon (2022) 14:4633–4646
https://doi.org/10.1007/s12633-021-01260-8

ORIGINAL PAPER

Current Transport, Photosensitive, and Dielectric Properties of *PVA/n-Si* Heterojunction Photodiode

A. Ashery[1] · A. E. H. Gaballah[2] · G. M. Turky[3]

Received: 7 May 2021 / Accepted: 4 July 2021 / Published online: 12 July 2021

Abstract

The results showed that the annealing of polyvinyl alcohol (*PVA*) at 450 K has improved its electrical conductivity. Scientists had previously overlooked its great characteristics because of its insulating properties however, *PVA* showed a considerable increase in conductivity, making it a promising material for optoelectronic devices. The electrical and dielectric properties of *PVA/n-Si* heterostructure were investigated. The ideality factor, barrier height, and series resistance were measured at different temperatures using various approaches as Nord, Chueng, and the conventional method. A detailed analysis of Ac conductivity, real and imaginary parts of the impedance (Z', Z") were examined at different temperatures, voltages, and frequencies. The results showed that the value of the imaginary part of the impedance Z" changes with temperature, voltage, and frequency; however, the novelty here is that Z" only takes positive values if the frequency is set to a very low value, such as 10 Hz. The photocurrent properties were also studied confirming that PVA/n-Si structure is responsive to daylight illumination.

Keywords PVA/n-Si heterojunction diode · I-V and C-V characterization · AC conductivity · Impedance spectroscopy

1 Introduction

Recently, Metal-Semiconductor (*MS*) structures with interface thin films for example polymers or an oxide such as Metal-Polymer-Semiconductor (*MPS*) or metal – oxide – semiconductor (MOS) have attracted great interest in the electronics and optics applications due to their interesting optoelectronic properties for instance very fast switching and very little forward-voltage [1, 2]. Organic and inorganic nanostructured materials have been purposely used in optoelectronic and electronic devices as novel nanocomposites, such as hybrid semiconductor films and polymer nanostructures in Schottky constructions [3–5]. Polymer thin film impurities can reduce the interface density of states, dislocations, and surface charges of the manufactured device, lowering its quality and sensitivity. [6–8]. Polyvinyl alcohol (*PVA*) has many advantages over conventional insulator thin films, including environmental friendliness, low coast content, low molecular weight, low-temperature processing, reliability, and ease of manufacture [9–12], it has low conductivity and great resistance compared to other polymeric material. The conductivity of *PVA* is due to physical interactions between the polymer chains and the bonding of hydrogen in the hydroxyl group as well as doping metals like Co, N, and Zn [13]. The efficiency of the Metal Polymer Semiconductors (MPS) depends on several parameters such as temperature, frequency, conduction mechanism, and barrier height (ϕ_b) at the metal semiconductors (MS) interface by taking into account the interfacial layer influences, series resistance (R_s), thin-film surface states located at the MS interface [14–17]. The dielectric and electrical characteristics of these structures are influenced by the MS barrier height, similarly, the (ϕ_b) of these structures has a substantial impact on transport conduction mechanisms [18]. According to reports, the conduction mechanism and the formation of ϕ_b can be adjusted by utilizing an appropriate middle thin film. Altındal et al. [19–21] have developed Al/SnO_2/p-Si (MOS) structures and studied their current-voltage (I-V) and capacitance-voltage (C-V) properties over a wide

✉ A. E. H. Gaballah
gaballah.nis@gmail.com

1 Solid-State Electronics Laboratory, Solid State Physics Department, Physics Research Division, National Research Centre, 33 El-Bohouth St., Dokki, Giza 12622, Egypt

2 Photometry and Radiometry Division, National Institutes of Standards (NIS), Tersa St, Al-Haram, Giza 12211, Egypt

3 Microwave Physics and Dielectrics Department, Physics Division, National Research Centre, Dokki, Giza 12622, Egypt

temperature range in order to assess the Rs and Nss impacts on them using an appropriate intermediate thin film. Demirzen et al. [22] developed Au/(BiPVA)/n-Si structures and examined their dielectric description. They showed that while dielectric constants and tanδ values are decreasing, σ_{ac}, M', and M" values are increasing with frequency increase. In this paper, we investigate the electrical and dielectric properties of pure polyvinyl alcohol (PVA), which has never been investigated before due to its low electrical conductivity. We improved its electrical conductivity by measuring the electrical properties at different temperatures up to 450 K as a result of annealing. The ideality factor, barrier height and series resistance of PVA/n-Si diode were investigated at different temperatures using several methods such as *I-V, H(I)-I, dv/dlnI-I*, and *F(V)-V*. Nyquist diagram, ac electrical conductivity, the real and imaginary parts of impedance (Z', Z") were studied at different temperatures, voltages, and frequencies. With changes in temperatures, voltages, and frequencies, Z" takes positive and negative values; however, the innovation here is that Z" only takes positive values if the frequency is set to an extremely low value, such as 10 Hz.

1.1 Experimental Procedure

An aqueous solution of highly concentrated polyvinyl alcohol was prepared, a few drops of PVA suspension were deposited on n-silicon wafer using spin coating technique after washing it with standard procedures to remove all contaminants and oxidized layer from the silicon surface. The thin film of PVA was dried for 30 min at 323 K, before being heated to 450 K for an hour. Two electrodes of gold (Au) and aluminum (Al) were deposited on the upper and lower surfaces of PVA/Si heterostructure diode respectively using the thermal evaporation technique. The conductivity of the resulted film has substantially improved as a result of the thermal treatment. Fig. 1a shows the X-ray diffraction pattern of Polyvinyl alcohol deposited on a glass substrate, it exhibits a distinct peak at 20°, indicating its semi-crystalline characteristics. The FTIR of *PVA* thin layer is seen in Fig. 1b, the spectrum shows the peak at 3300 cm^{-1} due to OH expanding of H-bonding; while the CO stretching peak for the alcohol group persists at 1200 cm^{-1}. FTIR spectrum of *PVA* displays a wide peak at about 3425 cm^{-1}, representing a widening of hydroxyl groups, the peak at 2950 cm^{-1} appears because of the stretching of C-H. The CH_2 extending mode for methylene groups remains at a peak of 1465 cm^{-1}. The surface topography of *PVA* was detected by the scanning electron microscope. Fig. 1c displays the *PVA* thin layer that had been inspected with magnifications of 1500. It can be detected from the SEM images that the current sample has a large smooth area, which reveals the creation of a clear and transparent-*PVA* film.

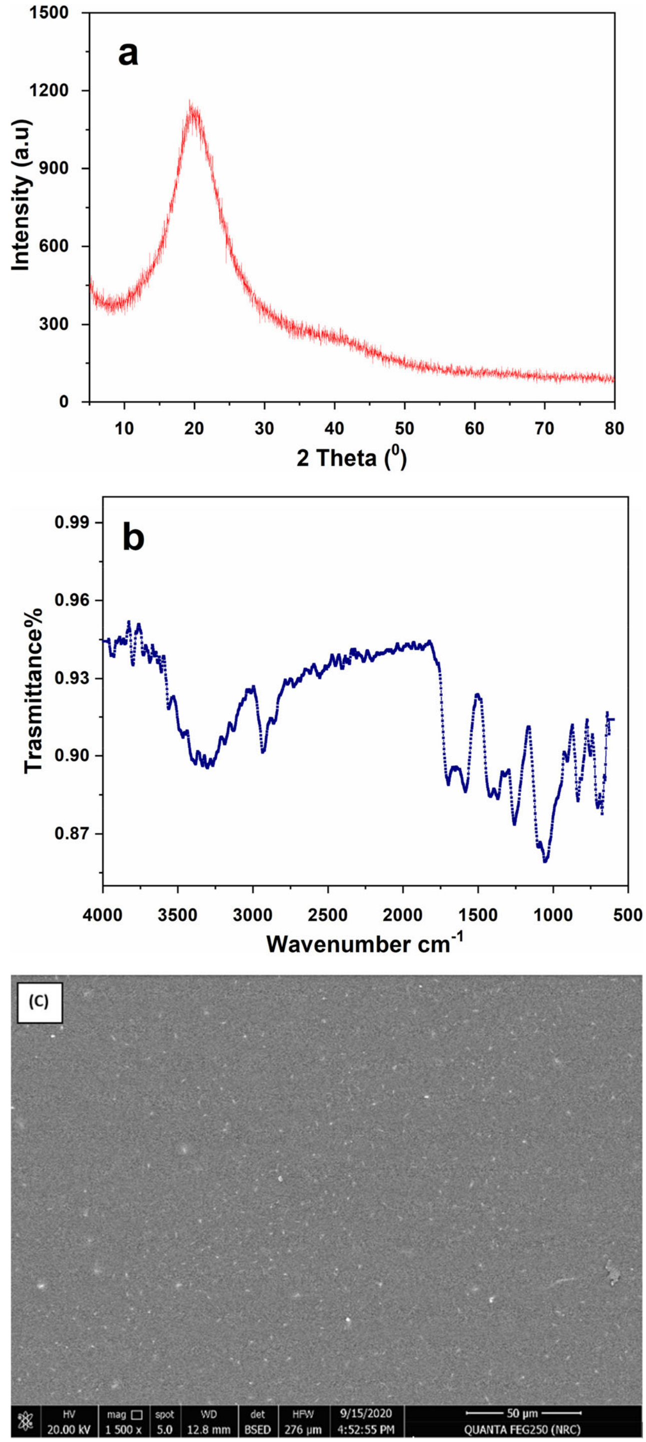

Fig. 1 **a, b, c** X-Ray diffraction pattern, FTIR, and SEM image of annealed *PVA* respectively

1.2 Electrical Properties

To obtain a clear view of the current conduction mechanism in detail, the I-V measurements were performed using KEYSIGHT B 2901A and the dielectric properties were measured in the frequency range 10 Hz–20 MHz and at a temperature range from 233 to 363 K using a Novocontrol highresolution alpha analyzer. The double logarithmic ln(I)-ln(V) diagram of the Au/PVA/n-Si/Al diodes were measured at different temperatures to understand the conduction mechanism as shown in Fig. 2(a, b). The I-V characteristics are found to behave similarly at all temperatures, and the current flows through the device increases as the temperature rises, the graphs show the power-law relationship between current and applied voltage (I α V ^{m}) with dissimilar values of the exponent (m) where m is the slope which can be determined from the linear part of the ln(I) vs. ln(V) curves. It is reported that for wide bandgap heterojunction diodes if the I-V plot follows the relation I exp. V, the dominated mechanism will be the recombination tunneling, however, it can be seen from Fig. 2(a,b) that I-V curves follow the power law, and hence the possibility of recombination-tunneling mechanism, in this case, is ruled out. The scheme comprises two separate linear regions (region I and II) with dissimilar slopes, the power-law (I α V ^{m}) can be fitted separately for the two regions. The basic mechanism in the first part agrees with be Ohm's law in case the slopes close to unity. The Ohmic contact is due to the bulk-produced current in the film prevailing over the injected free carrier-produced current. The values of the obtained slopes in the second part were 2.3 and 2.9 for the diodes, respectively. Exponents greater than two have previously been interpreted as a hint of trapped charge current with exponent trap spreading. As a result, the charge transference mechanism for diodes might be governed by the space charge current with exponentially distributed surface states [23, 24]. When the voltage is increased, the injection of electrons from the electrode to the films increases as well, according to the space charge limited conduction (SCLC) mechanism [26].

$$n\,(T) = \quad n_0 + \quad T_0/T \tag{1}$$

As shown in Fig. 3, the ideality factor changes nearly linearly with the reverse temperature as anywhere n0 and T0 are constants, which were found to be 2.27 and 381.7 K respectively. The temperature dependence of n suggests that the current conduction mechanism is controlled by the thermionic field emission (TFE) [25–27].

To explore the temperature dependence of (n), a plot of n vs. $1/T$ is shown in Fig. 3. The value of n is closer to unity at high temperatures, and n increases with decreasing temperature. The additional explanation could be credited to the inhomogeneities of the diodes for such temperature dependence of n [28–30]. Also, the n values are not fixed with temperature, they are detected linearly with the temperature reverse ($1/T$), as realized in Fig. 3. The potential barrier ϕ_b vs. n is demonstrated at different temperatures in Fig. 4. There is a linear relationship between the ϕ_b and n, which has been explained

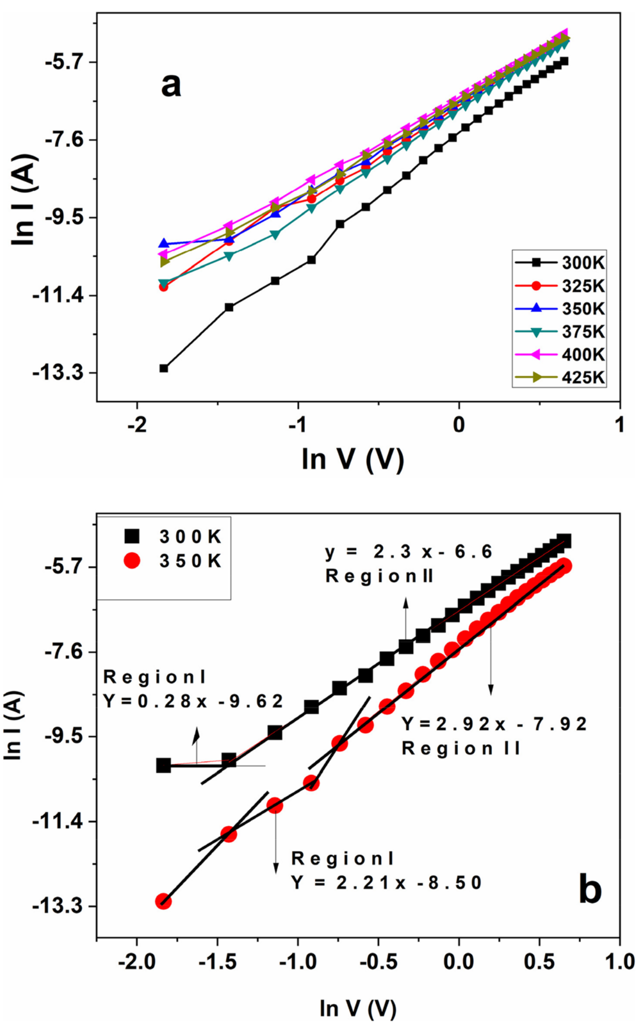

Fig. 2 **a, b** ln I versus ln V at different temperatures for *Au/PVA/n-Si/Al* diode

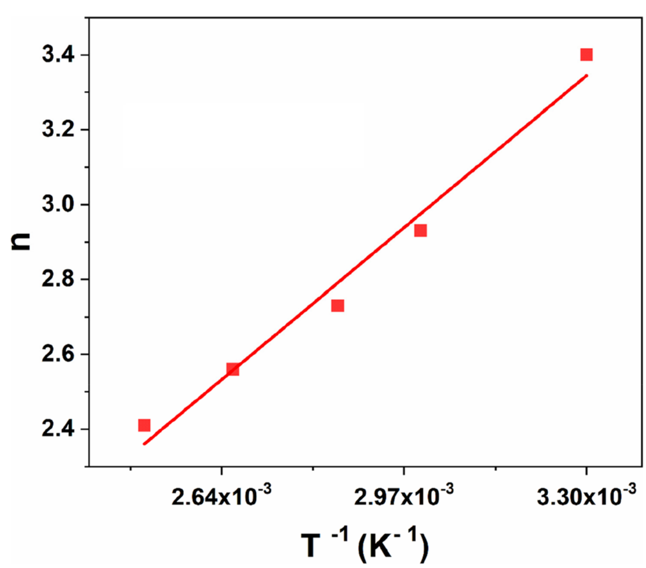

Fig. 3 Ideality factor (n) vs T^{-1} at different temperatures for *Au/PVA/n-Si/Al* diode

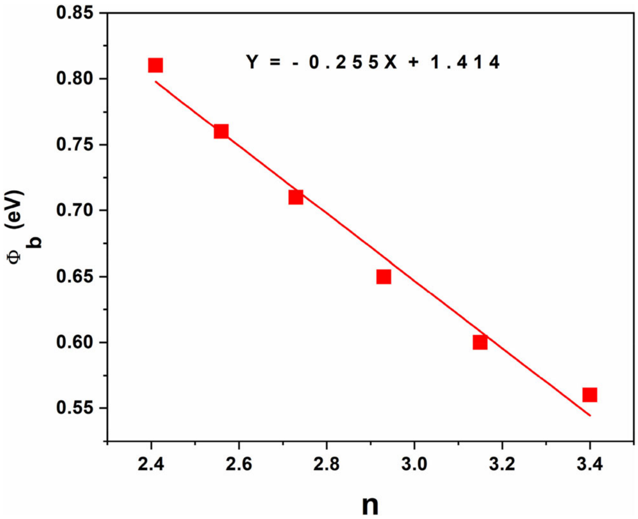

Fig. 4. ϕ b vs *n* at different temperatures of *Au/PVA/n-Si/Al* diode

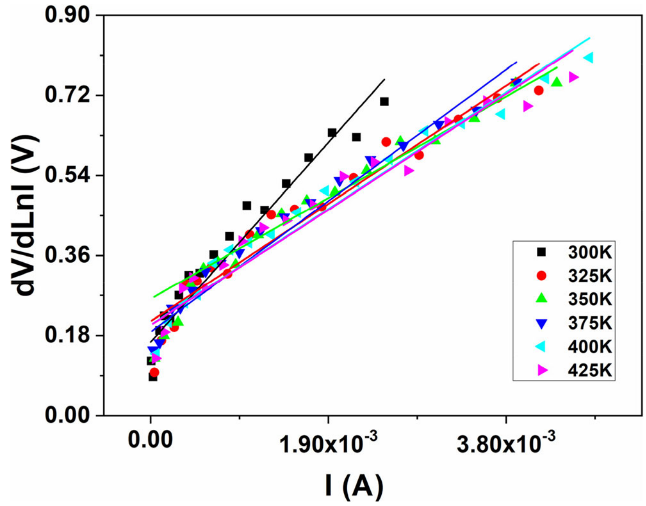

Fig. 5. *dv/dlnI* vs *I* at different temperatures of *Au/PVA/n-Si/Al* diode

by lateral inhomogeneities of *Au/PVA/n-Si/Al*. The extrapolation of the ϕ_b vs. n figure to $n = 1$ has given a homogeneous structure of about 1.41 eV.

The series resistance R_s and other parameters such as (n) and ϕ_b were also determined through Cheung's functions [31–33]. Regarding the Cheung, the forward bias *I-V* characteristics of a diode can be expressed as:

$$I = I_0\left[exp\ \frac{q(V - IR_s)}{nkT}\right] \tag{2}$$

wherever IR_s term is the voltage drop across the diode because of R_s. its value can be determined from the subsequent equation as:

$$\left(\frac{dV}{dlnI}\right) = \frac{nkT}{q} + IR_s \tag{3}$$

$$H(I) = V - n\left(\frac{KT}{q}\right)Ln\left(\frac{I}{AA^*T^2}\right) \tag{4}$$

and *H(I)* is assumed as follows

$$H(I) = n\varphi_b + IR_s \tag{5}$$

A plot of *dV/dln (I)* against I will give R_s values as the slope and nkT/q as the intercept of the y-axis according to Eq. (3). Fig. 5 displays *dV/dln(I)* vs I for *Au/PVA/n-Si/Al* diode at different temperatures as 300, 325,350,375,400, and 425 K respectively, and the values of R_s are listed in Table 1.

Fig. 6. shows the plot of *H (I)* vs *I*, it gives a straight line with y-axis intercept equal to $n\Phi_b$, while the slope gives another determination of R_s. The output parameters of the barrier height values and R_s are listed in Table. 1.

Table. 1 presents different values of the ideality factor (n), the variation of (n) may be attributed to the effects of series resistance and the bias dependency of diodes, resulting in the voltage drop across the interfacial thin film and charge of the interface states with the bias in the low voltage region of the I-V diagram [31–34]. To compare the active barrier height of *Au/PVA/n-Si/Al* diode, the Norde method is adopted as the high R_s can cause a precise evolution of barrier height from the standard *ln (I)-V* Fig. [35]. In this way, the function *F(V)* is drawn against voltage. The function *F(V)* is assumed by

$$F(V) = \frac{V}{\Upsilon} - \frac{1}{\beta}Ln\left(\frac{l}{AA'T^2}\right) \tag{6}$$

Where $\beta = q/KT$ and Υ is a factor ≤ the ideality factor (n), the active barrier height is given by

$$\varphi_b = F(V_{min}) + \frac{V_{min}}{\Upsilon} - \frac{1}{\beta} \tag{7}$$

where $F(V_{min})$ is the minimum value of *F(V)* corresponding to V_{min}. The plot of F(V) against V for the *Au/ PVA/n-Si/Al* diode at different temperatures is seen in Fig. 7. The output parameters are listed in Table. 1, these values are in good agreement with those obtained from *ln (I)-V* method.

Figure 8 shows the current (I)–time (t) graph of PVA/n-Si photodiode characterized under daylight illumination of 60 mW/cm^2. The photocurrent was observed when the light is switched on; contrary when the light is switched off, a rapid decrease in the photocurrent is observed [36]. It was confirmed that PVA/n-Si diode is responsive to daylight illumination. The photodiode response to daylight illumination indicates that photodiodes have the potential to be used as solar detectors.

1.3 Dielectric Properties

The variation of the real and imaginary parts of impedance (Z', Z") with frequency at various voltages and

Table. 1 The calculated ideality factor, barrier height, and series resistance of *Au/PVA/n-Si/Al* at different temperatures using different methods

T (K)	(I-V)			Cheung (H)			Cheung (dV/dlnI)		Norde (F)		
	n	Φ_b eV	$R_s \Omega$	n	Φ_b eV	$R_s \Omega$	n	$R_s \Omega$	n	Φ_b eV	$R_s \Omega$
300	3.40	0.56	5.6×10^{2}	2.39	5.8×10^{-1}	5.8×10^{3}	2.39	8.98×10^{3}	3.40	5.01×10^{-3}	1.25×10^{-1}
325	3.15	0.60	3.36×10^{2}	2.22	6.69×10^{-1}	5.8×10^{3}	2.22	8.98×10^{3}	3.15	1.62×10^{-3}	5.01×10^{-3}
350	2.93	0.65	3.22×10^{2}	2.06	7.16×10^{-1}	5.8×10^{3}	2.06	8.98×10^{3}	2.93	5.01×10^{-3}	1.91×10^{1}
375	2.73	0.71	3.0×10^{2}	1.92	7.63×10^{-1}	5.8×10^{3}	1.92	8.98×10^{3}	2.73	5.01×10^{-3}	2.11×10^{1}
400	2.56	0.76	2.87×10^{2}	1.80	8.1×10^{-1}	5.80×10^{3}	1.80	8.98×10^{3}	2.56	5.01×10^{-3}	2.24×10^{1}
425	2.41	0.81	2.17×10^{2}	1.70	8.56×10^{-1}	5.80×10^{3}	1.70	8.98×10^{3}	2.41	5.01×10^{-3}	2.33×10^{1}

temperatures was demonstrated in Fig. 9(a,b,c,d,e,f). The values of Z' almost zero at high and mid frequencies, while at low frequencies the values of Z' rise and scatter into curves for each voltage due to the presence of structural special effects as pores, grains, surface morphology, and polarization [37]. The values of Z' change with the following temperatures (300, 360, 223 K) as (37×10^{3}, 15×10^{3}, 85×10^{3}) respectively. The values of Z' increase with reducing temperatures and reached their maximum values at a negative temperature as shown in Fig. 9(a,b,c). The decrease in impedance (Z') with an increase in frequency and temperature means the possibility of AC conductivity growth. [38]. Z" remains without change at high frequencies and its values equal zero, while at mid-frequency, Z" decreased and formed many peaks for each voltage takes negative values, in low frequencies Z" rise and takes positive voltages. As shown in Fig. 9(d,e,f), the values of Z" rise with reducing temperatures and reach their maximum at a negative temperature as the following (300,360,223)K (13×10^{3}, 5×10^{3}, 25×10^{3}).

Figure 10 (a,b,c,d,e,f) display the variation of Z',Z" with frequency at different temperatures and voltages for *PVA/n-Si* structure. Z' remains constant without any change at high frequencies, but Z' scattered in curves for each temperature at mid frequencies, Z 'values increase with decreased temperatures, Z' values change with voltages as (5×10^{3} to 7×10^{4}, 5×10^{3} to 4×10^{4}, 2×10^{3} to 32×10^{3}) for applied voltage (0, 2, − 2 V) respectively as shown in Fig. 10(a,b,c). The change in Z' at high frequencies designates the existence of a probable release of charge polarization due to the decrease in the barrier of material with the rise of temperature [39]. It noted that with increasing temperature, the Z' increases and decreases once the temperature rises, a major decrease in the boundaries of grains and grains. Z" constant at high frequencies, curves for each temperature developed at mid frequencies, indicating the existence of the relaxation technique in the system. The relaxation happens due to the existence of immobile species at little temperatures and imperfections and vacancies at higher temperatures [40], the Z" rise with decreased temperatures taking negative values and rises to positive values at low frequencies, the variation of Z" with the voltages as the following (0, 2, − 2) V (-3×10^{4}–2.5×10^{4}, -2×10^{4}–1.5×10^{4}, -1.5×10^{4}–1.2×10^{4}) respectively.

Figure 11(a,b,c,d,e,f) display voltage and temperature dependence of Nyquist figures (fitted complex impedance spectrum) at certain selected temperatures and voltages as the follows (2 V to -2 V), (223 K to 363 K) respectively, the complex impedance equation is expressed as

$$Z^{*} = Z^{`}(\omega) + iZ^{``}(\omega) \tag{8}$$

where,

$$Z^{`} = \frac{R_g}{1+\omega_g^2 C_g^2 R_g^2} + \frac{R_{gb}}{1+\omega_{gb}^2 C_{gb}^2 R_{gb}^2} \tag{9}$$

$$Z^{``} = \frac{-R_g^2 \omega_g C_g}{1+\omega_g^2 C_g^2 R_g^2} + \frac{-R_{gb} w_{gb} C_{gb}}{1+\omega_{gb}^2 C_{gb}^2 R_{gb}^2} \tag{10}$$

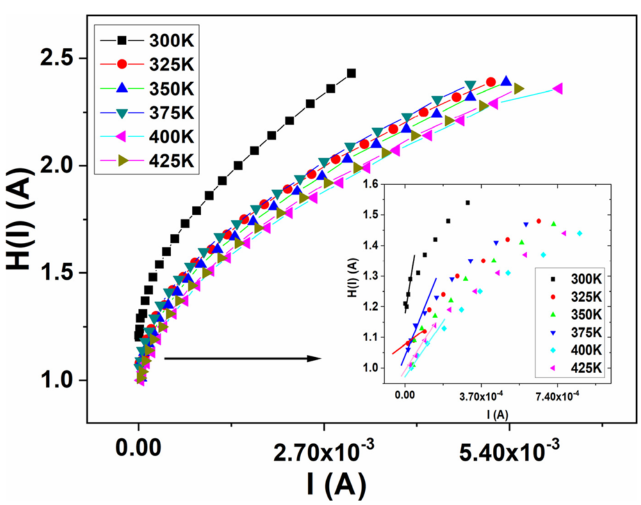

Fig. 6. *H (I)* vs *I* at different temperatures of *Au/PVA/n-Si/Al* diode

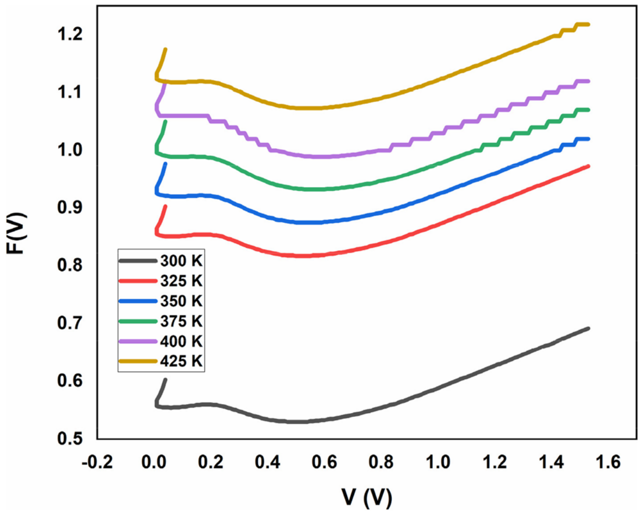

Fig. 7. *F (V)* vs *V* at different temperatures of *Au/PVA/n-Si/Al* diode

It can be shown that the complex impedance systems are depressed and that the center of the semicircle lies under the actual (Z”) axis, which accepts the multi-dispersive (multi-Debye type) nature of dielectric relaxation in *Au/PVA/n-Si/Al.* This may be attributed to the presence of dispersed components in the material-electrode phase. These depressed semicircles are not caused by imperfections or by interfacial capacitance. These may be due to the relaxation times that are presumed to be superimposed with the actual reaction of the structure [41, 42]. The arcs correspond to the response of the bulk of the structure grains at the high-frequency end and the small frequency arcs agree to the effects of the grain border [43–45]. Rising temperatures and voltages in the system at higher temperatures and voltages are detected as decreases in the zone of the semicircle.

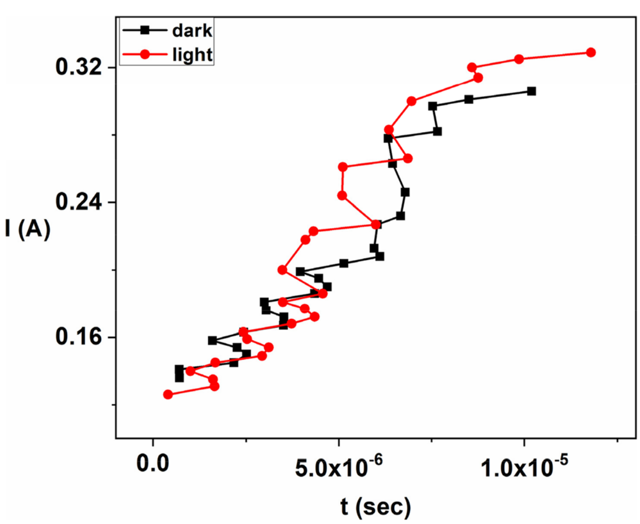

Fig. 8 The current (I)–time (t) graph of PVA/n-Si photodiodes

Figure 12 (a,b,c,d,e,f) display the variation of Z’, Z” as a function of voltage at different frequencies and constant different temperatures. Z’ increases in the positive region of the voltage also increase with decreasing frequencies forming two peaks, these two peaks appeared in Z” similar to the behavior of Z’, but Z’ takes positive values, while Z” takes positive values at low frequencies and negative values at high frequencies as displayed in Fig. 12(a,d). In Fig. (b,e), Z’, Z” take the same manner in the positive values near the zero value, but Z” takes positive values at low frequencies and negative values at high frequencies as shown in Fig. 12 (e), also the behavior of Z’, Z” seen in the Fig (c,f) is similar to its manner in Fig. 12(b,e).

Figure 13(a,b,c,d,e,f) display the variation of Z’,Z” as a function of temperature at different frequencies and constant voltages. Z” increase with frequencies, while Z’ increase with decreasing frequencies, Z’, Z” rise with decreasing temperatures, especially at low temperatures. Z” takes positive values at low frequencies, while at high frequencies takes negative values, Z’, Z” increases with decreasing voltage as shown in Fig. 13(a,b,c,d,e,f).

Figure 14(a,b,c,d,e,f) display the variation of Z’, Z” as a function of voltage at different temperatures and constant frequency of *Au/PVA/n-Si/Al.* The values of Z’ rise with decreasing temperature, especially at low temperatures. It is worthy noted that Z’ values increase with reducing frequency as follows (2×10^7, 10^3,10) Hz, (18–30, 3×10^3–25×10^3, 10^3–8×10^4) respectively. Here we can say that by variation of frequency we can tune the impedance value as shown in Fig. 14(a,b,c). Z” increases with decreasing temperatures, but at the low frequency of 10 Hz, Z” takes positive values and its manner is similar to that of Z’ as shown in Fig.14(a,d). By increasing frequency to 10^3 Hz, Z” values take negative values and its manner is contrary to that of Z” at 10 Hz, with increasing frequencies Z” at low frequencies takes positive values, but at high frequencies takes negative values as shown in Fig. 14 (d,e,f), but its values increase with decreasing frequencies .from mention above we can tune the values of Z’, Z” by variation of temperature and frequency

Figure 15 (a,b,c,d) illustrates the temperature dependence of AC conductivity of the *Au/PVA/n-Si/Al* film at different voltages and constant frequencies. AC conductivity is expressed by the equation:

$$\sigma_{tot} = \sigma_0(T) + A\omega^s \qquad (11)$$

The AC conductivity increases with temperature and its values rise with frequencies as shown in Fig. 15 (a,b,c). Moreover, the movement of the space charges becomes

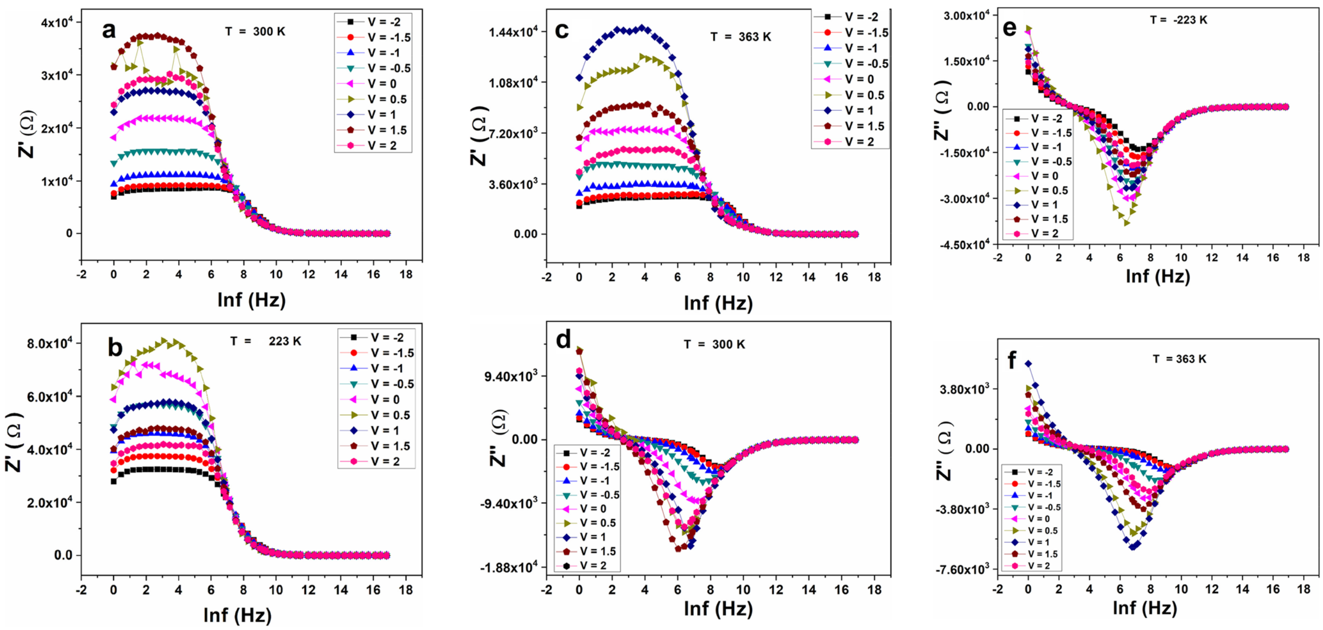

Fig. 9 **a**, **b**, **c** Z' vs f at different voltages and T = 30C°,-50, 90 respectively, **d**, **e**, **f** Z" vs f at different voltages and T = 30C°,-50, 90 respectively

easier, resulting in a rapid increase in conductivity. Fig. 15d displays $\ln\sigma_{ac}$ against *1000/T*, each curve has two straight line regions, the activation energy (E_a) values were obtained from the slop at dissimilar voltages as seen Fig. 15d. The activation energy is raised with growing voltage. The higher activation energy that is detected in the high-temperature area might be due to the summation of energies required for the generation of charge carriers and their motion into vacancies [46, 47].

The electrical conductivity σ_{ac} and $\ln\sigma_{ac}$ of *Au/PVA/n-Si/Al* heterojunction diode was examined as a function of frequency in a wide range of voltages (-2 V to 2 V) and different temperatures. The σ_{ac} versus frequency at different voltages is seen in Fig. 16 (a,b,c,d,e,f), it can be seen that the electrical conductivity at each voltage has two characteristic regions, the primary one is frequency independent section and called dc conductivity comparatively in low frequencies. In this section, σ_{ac} does not

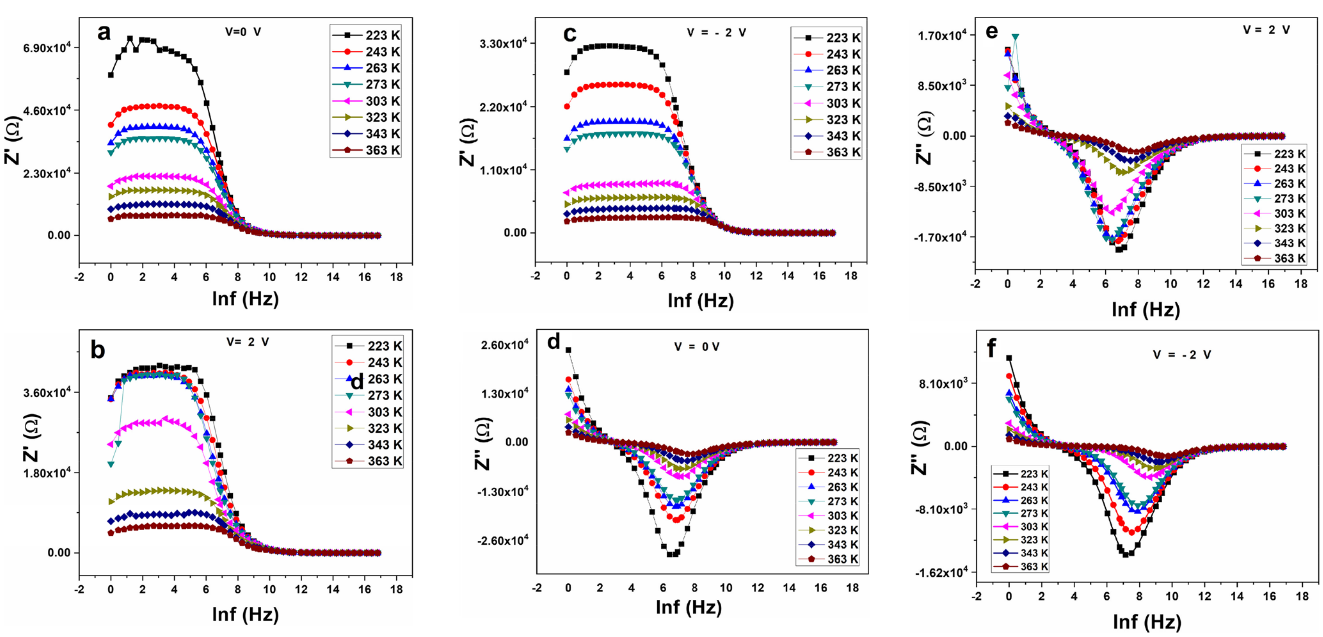

Fig. 10 **a, b, c** Z' vs f at different temperatures and V = 0,2,-2 v respectively, **e, f, g** Z" vs f at different temperatures and V = 0,2,-2 V respectively

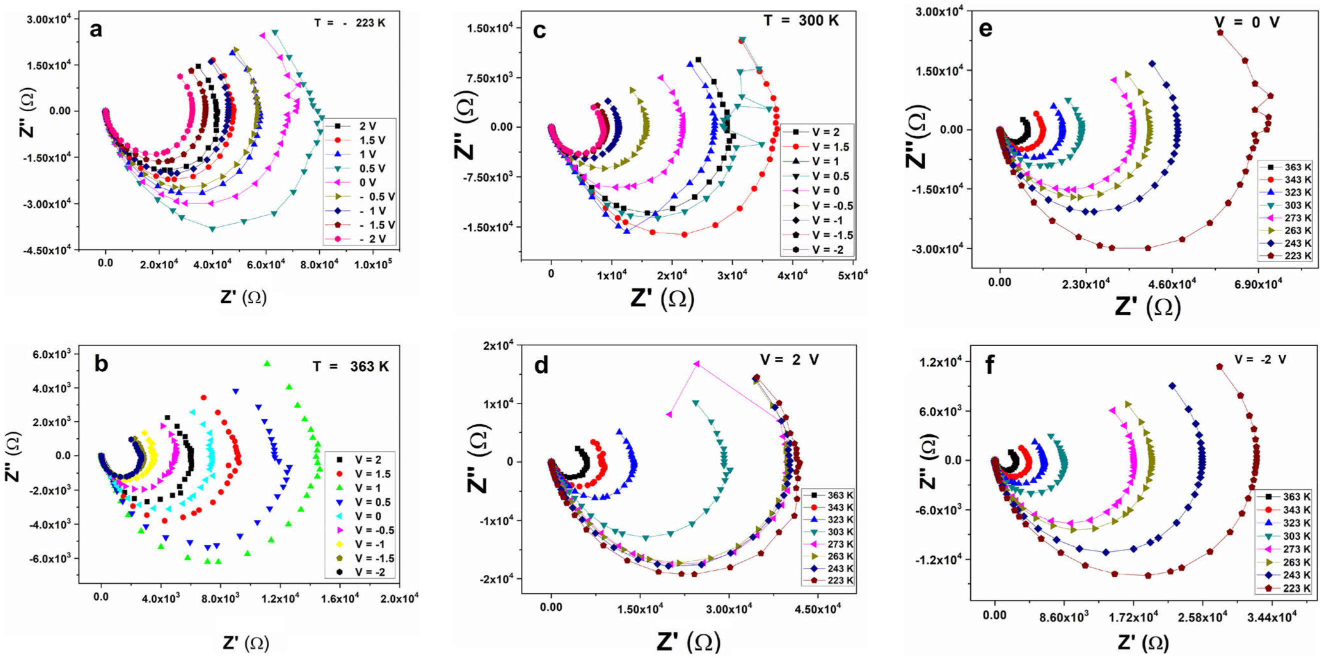

Fig. 11 **a**, **b**, **c** Nyquist curves of Au /PVA/n-Si/Al at different voltages and fixed temperatures, **d**, **e**, **f** at different temperatures and fixed voltages

change with frequency, furthermore, it is understood that the frequency self-governing section extends through the upper frequencies with growing voltage values. The second part of the σ_{ac} is frequency-dependent and this region is called ac conductivity. In this section, the conductivity increases with increasing frequency. Also, both ac and dc conductivities rise with increasing voltage as seen in Fig. 16 (d,e,f). Those are created by different mechanisms of charge transport depending on frequency and voltage factors. Here is a transition section between

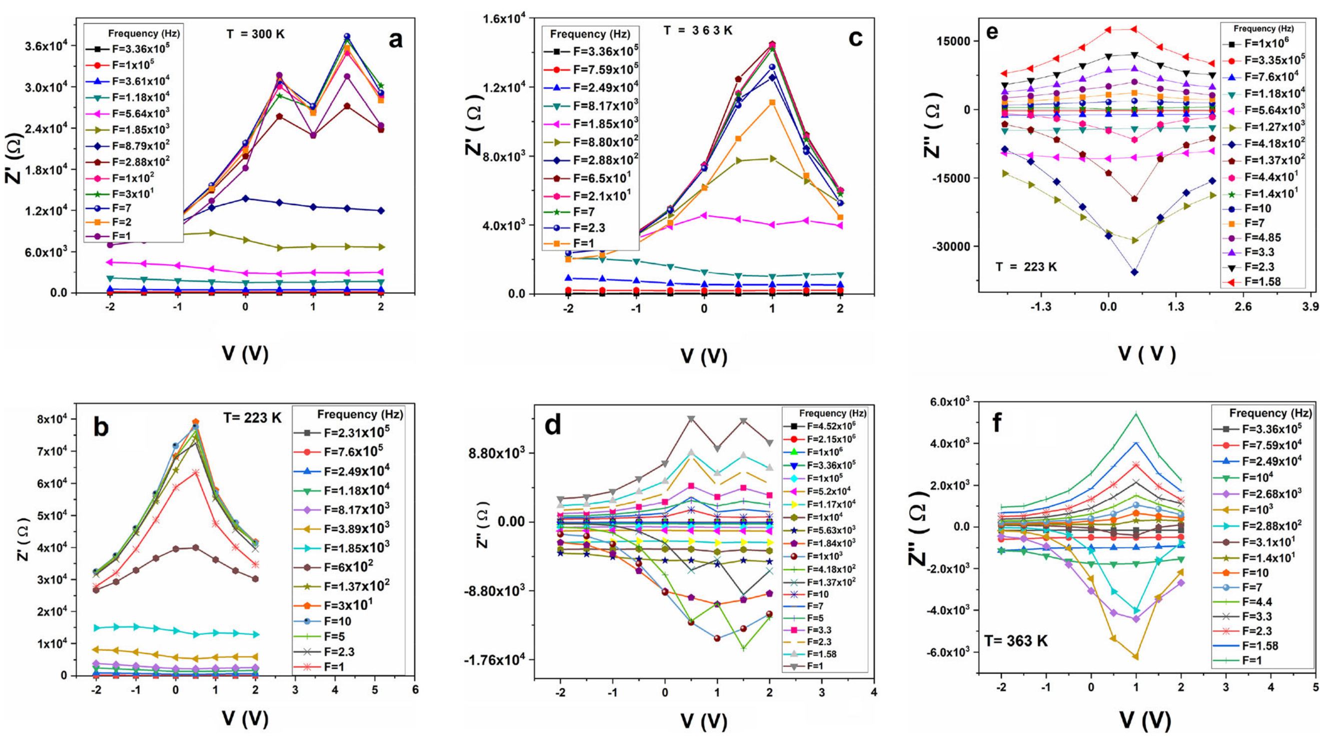

Fig. 12 **a**, **b**, **c** Z' vs v at different frequencies and T = 30,-50,90 c° respectively, **d**, **e**, **f** Z'' vs V at different frequencies and T = 30,-50,90 c° respectively

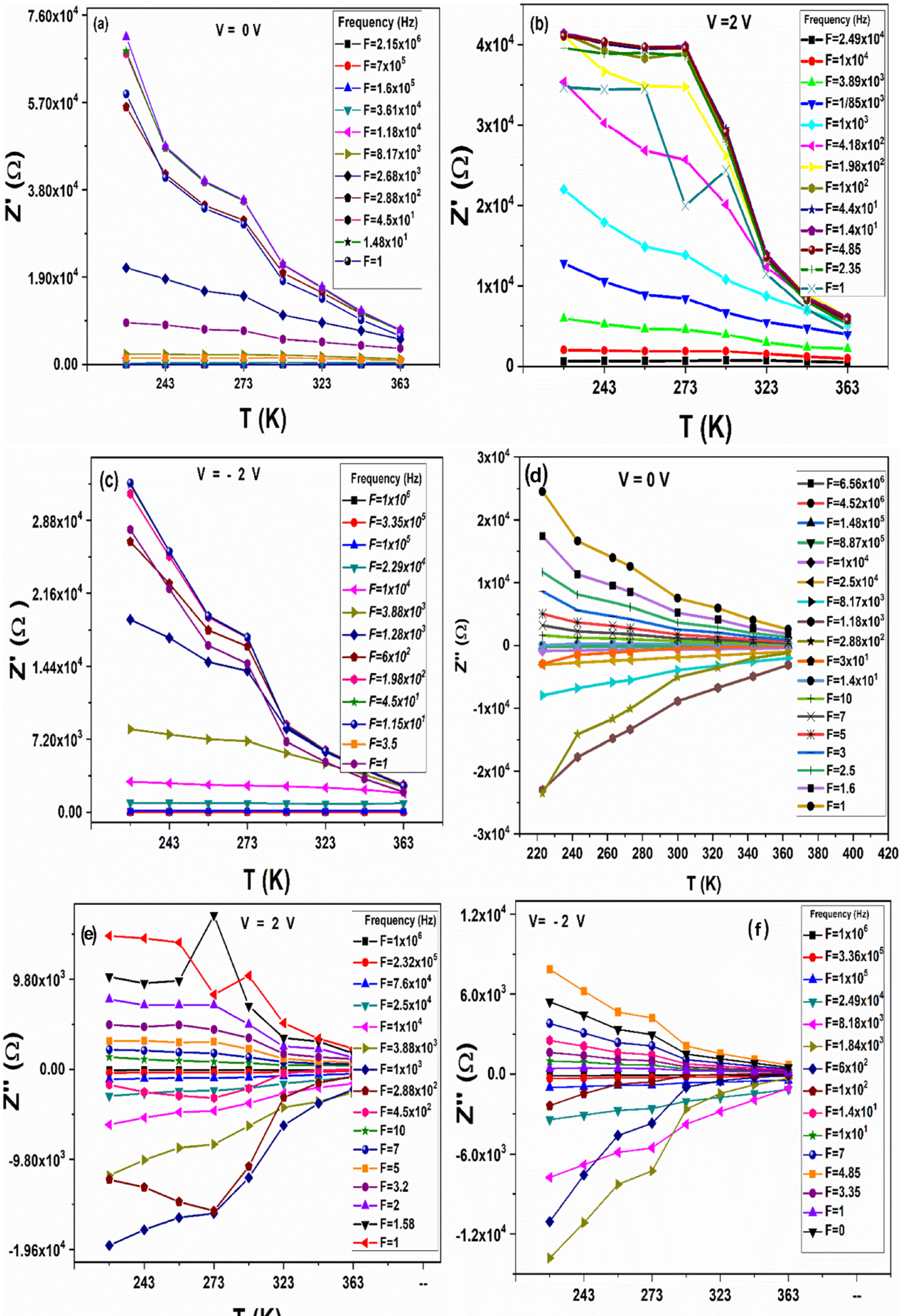

Fig. 13 **a**, **b**, **c**, **d**, **e**, **f** Z` Z`` vs T at different frequencies and voltages V = 0,2,-2 V respectively

those lined regions. The slope of those lined sections provides us exponent s factor and this temperature reliant on exponent s conduct clarifies us which transport mechanism takings place in the structure [48].

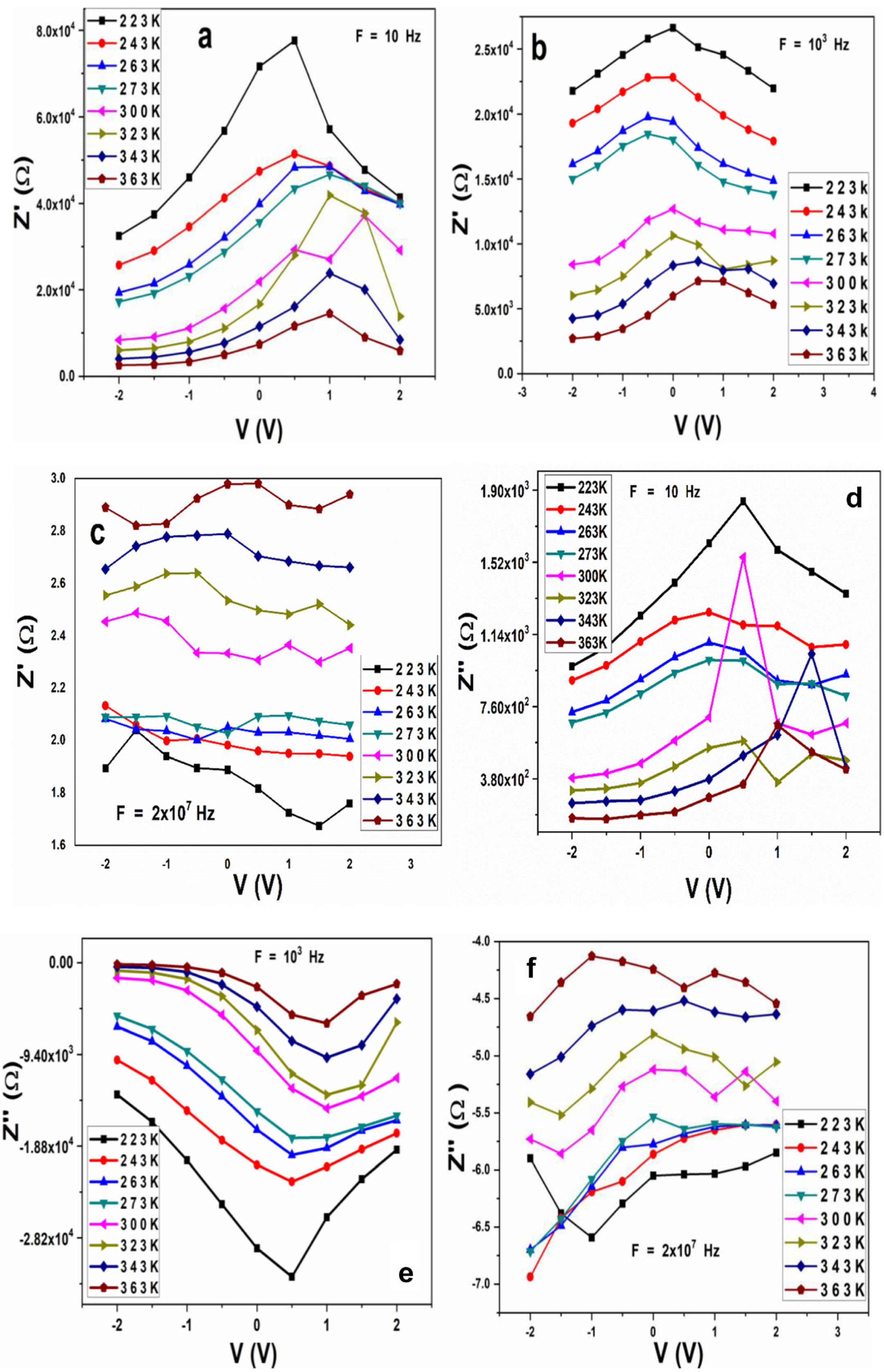

Fig. 14. **a**, **b**, **c**, **d**, **e**, **f** Z` Z`` vs V at different temperatures and f = 10,103,2 × 107 respectively

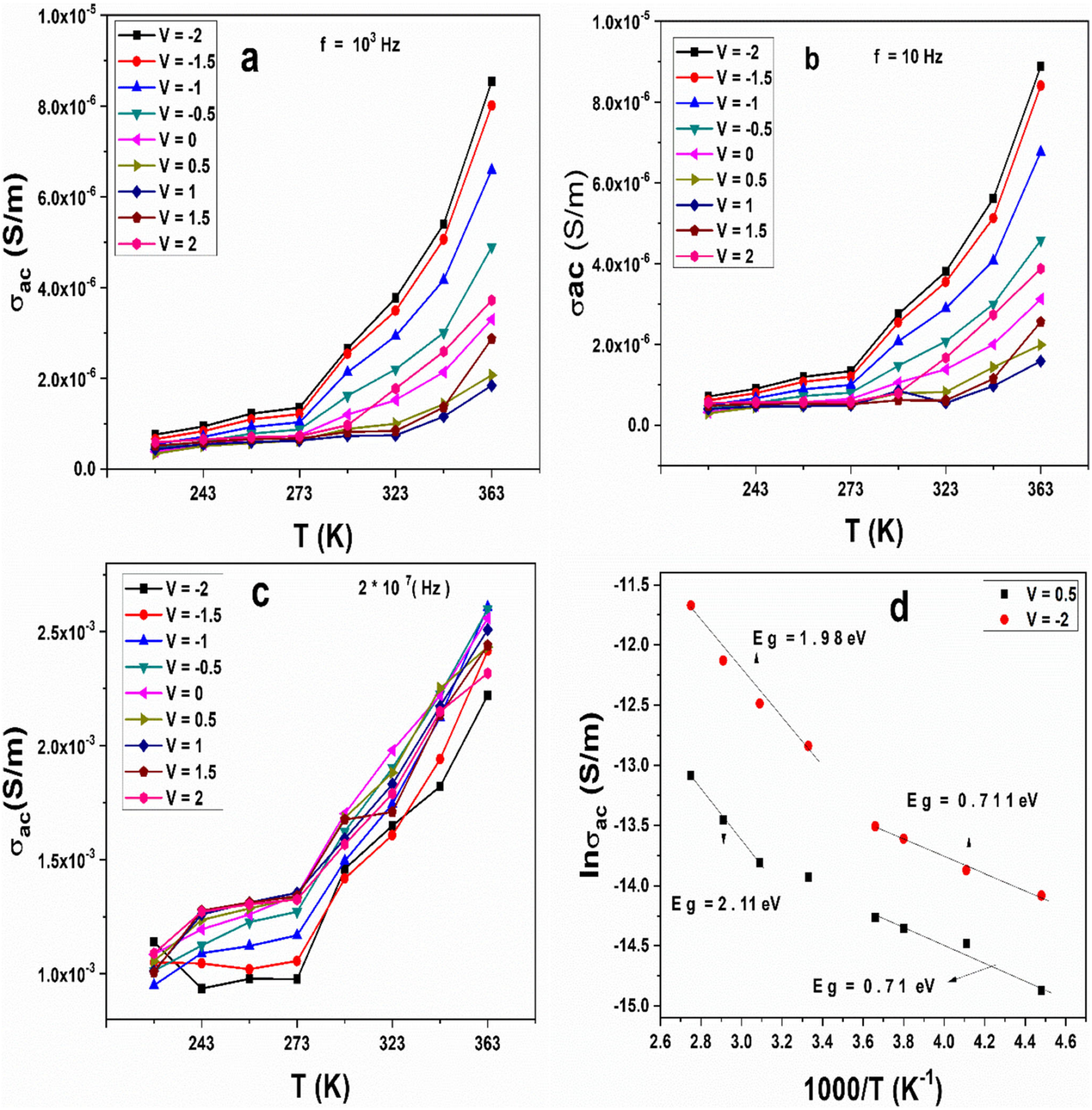

Fig. 15 **a, b, c** σ ac versus T at different voltages and constant frequencies,14d) lnσac versus *1000/T* at voltages 0.5 V, -2 V

2 Conclusion

We reported that annealing of PVA at 450 K greatly enhances its electrical conductivity, making it a viable material for electronic device manufacturing. We deposited polyvinyl alcohol (PVA) on silicon wafer using spin coating technique, and studied its electrical and dielectric properties. The ideality factor, barrier height, and series resistance were investigated at different temperatures by using different approaches as I-V, H(I), dv/dlnI-I, and F(V). With the change of temperature, voltages, and frequency, the Nyquist diagram, Ac electrical conductivity, and real and imaginary components of the impedance (Z', Z") were completely explored. The value of the imaginary component of the impedance (Z") can be positive or negative, but the novelty here is that Z" can only be positive if the frequency is set to an extremely low value, such as 10 Hz. In addition to that, it was confirmed that PVA/n-Si

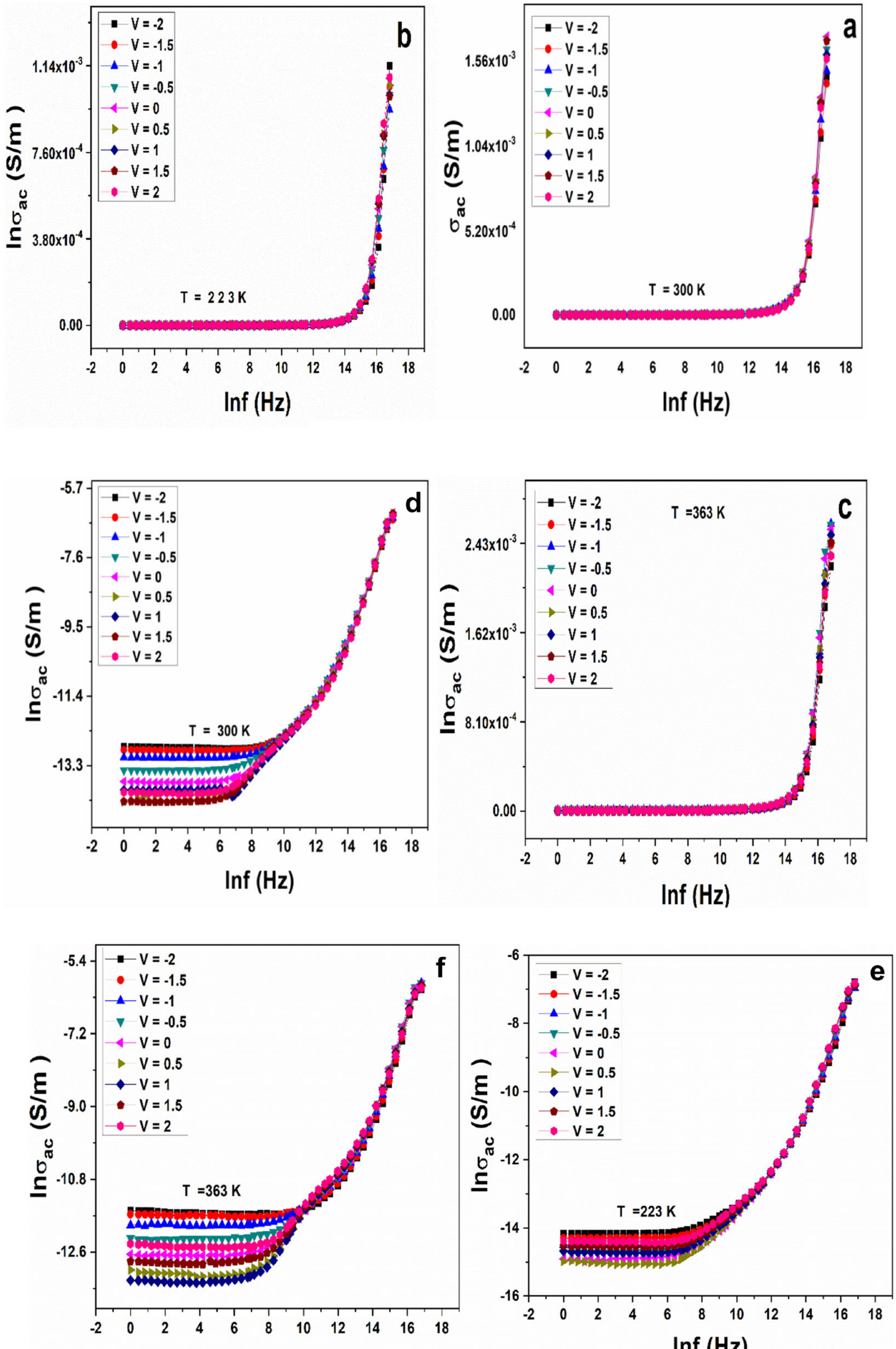

Fig. 16 **a, b, c** σac versus lnf at different voltages and fixed temperatures, (**e, f, g**) lnσac versus lnf at different voltages and fixed temperatures

photodiode is responsive to daylight illumination where the photocurrent was observed when the light is switched on; and a rapid decrease in the photocurrent occurred when the light is switched off.

Acknowledgments This work was supported by Ministry of Higher education and scientific research of Egypt.

Author Contributions All authors have contributed equally to the work.

Funding The authors received no financial support for the research, authorship, and publication of this article.

Data Availability Data sharing not applicable.

Declarations applicable.

Consent to Participate Informed consent was obtained from all individual participants included in the study.

Consent for Publication agree.

Conflict of Interest The authors declare no conflicts of interest associated with this manuscript.

References

1. Bilkan Ç, Azizian-Kalandaragh Y, Altındal Ş, Shokrani-Havigh R (2016) Frequency and voltage dependence dielectric properties, ac electrical conductivity and electric modulus profiles in Al/Co3O4-PVA/p-Si structures. Phys B Condens Matter 500:154–160. https://doi.org/10.1016/j.physb.2016.08.001
2. Baraz N, Yücedağ İ, Azizian-Kalandaragh Y, Ersöz G, Orak İ, Altındal Ş, Akbari B, Akbari H (2017) Electric and dielectric properties of au/ZnS-PVA/n-Si (MPS) structures in the frequency range of 10–200 kHz. J Electron Mater 46:4276–4286. https://doi.org/10.1007/s11664-017-5363-6
3. Bilkan Ç, Altındal Ş, Azizian-Kalandaragh Y (2017) Investigation of frequency and voltage dependence surface states and series resistance profiles using admittance measurements in Al/p-Si with Co3O4-PVA interlayer structures. Phys B Condens Matter 515: 28–33. https://doi.org/10.1016/j.physb.2017.04.002
4. Bilkan Ç, Badali Y, Fotouhi-Shablou S, Azizian-Kalandaragh Y, Altındal Ş (2017) On the temperature dependent current transport mechanisms and barrier inhomogeneity in au/SnO2–PVA/n-Si Schottky barrier diodes. Appl Phys A Mater Sci Process 123:560. https://doi.org/10.1007/s00339-017-1168-y
5. Ashery A, Gad S, Shaban H, Gaballah AEH (2021) Heterostructure device based on Graphene oxide/TiO2/n-Si for optoelectronic applications. ECS J Solid State Sci Technol 10:021002. https://doi.org/10.1149/2162-8777/abe1d9
6. Siva Pratap Reddy M, Sreenu K, Rajagopal Reddy V, Park C (2017) Modified electrical properties and transport mechanism of Ti/p-InP Schottky structure with a polyvinylpyrrolidone (PVP) polymer interlayer. J Mater Sci Mater Electron 28:4847–4855. https://doi.org/10.1007/s10854-016-6131-8
7. Badran RI, Umar A, Al-Heniti S et al (2010) Synthesis and characterization of zinc oxide nanorods on silicon for the fabrication of p-Si/n-ZnO heterojunction diode. J Alloys Compd 508:375–379. https://doi.org/10.1016/j.jallcom.2010.08.048
8. Azizian-Kalandaragh Y, Khodayari A, Behboudnia M (2009) Ultrasound-assisted synthesis of ZnO semiconductor nanostructures. Mater Sci Semicond Process 12:142–145. https://doi.org/10.1016/j.mssp.2009.09.006
9. Mansour AF, Mansour SF, Abdo MA (2015) Improvement Structural and Optical Properties of ZnO / PVA Nanocomposites 7:60–69. https://doi.org/10.9790/4861-07226069
10. Samzadeh-Kermani A, Mirzaee M, Ghaffari-Moghaddam M (2016) Polyvinyl alcohol/Polyaniline/ZnO Nanocomposite: synthesis, characterization and bactericidal property. Adv Biol Chem 06:1–11. https://doi.org/10.4236/abc.2016.61001
11. Hu G, Zhou R, Yu R, Dong L, Pan C, Wang ZL (2014) Piezotronic effect enhanced Schottky-contact ZnO micro/nanowire humidity sensors. Nano Res 7:1083–1091. https://doi.org/10.1007/s12274-014-0471-6
12. Bacaksiz E, Aksu S, Çankaya G, Yılmaz S, Polat İ, Küçükömeroğlu T, Varilci A (2011) Fabrication of p-type CuSCN/n-type micro-structured ZnO heterojunction structures. Thin Solid Films 519: 3679–3685. https://doi.org/10.1016/j.tsf.2011.01.254
13. Vijaya Kumar G, Chandramani R (2010) Doping and irradiation dependence of electrical conductivity of Fe 3+and Ni2+ doped polyvinyl alcohol films. Acta Phys Pol A 117:917–920. https://doi.org/10.12693/APhysPolA.117.917
14. Rebaoui Z, Bachir Bouiajra W, Abboun Abid M, Saidane A, Jammel D, Henini M, Felix JF (2017) SiC polytypes and doping nature effects on electrical properties of ZnO-SiC Schottky diodes. Microelectron Eng 171:11–19. https://doi.org/10.1016/j.mee.2017.01.010
15. Ali GM, Chakrabarti P (2013) Fabrication and characterization of nanostructure thin film ZnO Schottky contacts based UV photodetectors. In: Proc.SPIE
16. Thuy Doan M, Vinh Ho X, Nguyen T, Nguyen VN (2014) Influence of doping co to characterization of ZnO nanostructures. Adv Nat Sci Nanosci Nanotechnol 5:25011. https://doi.org/10.1088/2043-6262/5/2/025011
17. Orak I, Kocyigit A, Alindal Ş (2017) Electrical and dielectric characterization of au/ZnO/n–Si device depending frequency and voltage. Chin Phys B 26:28102. https://doi.org/10.1088/1674-1056/26/2/028102
18. Opel M, Geprägs S, Althammer M, Brenninger T, Gross R (2013) Laser molecular beam epitaxy of ZnO thin films and heterostructures. J Phys D Appl Phys 47:34002. https://doi.org/10.1088/0022-3727/47/3/034002
19. Altındal Ş, Karadeniz S, Tuğluoğlu N, Tataroğlu A (2003) The role of interface states and series resistance on the I–V and C–V characteristics in Al/SnO2/p-Si Schottky diodes. Solid State Electron 47:1847–1854. https://doi.org/10.1016/S0038-1101(03)00182-5
20. Nikravan A, Badali Y, Altındal Ş, Uslu İ, Orak İ (2017) On the frequency and voltage-dependent profiles of the surface states and series resistance of au/ZnO/n-Si structures in a wide range of frequency and voltage. J Electron Mater 46:5728–5736. https://doi.org/10.1007/s11664-017-5613-7
21. Baraz N, Yücedağ İ, Azizian-Kalandaragh Y, Altındal Ş (2017) Determining electrical and dielectric parameters of dependence as function of frequencies in Al/ZnS-PVA/p-Si (MPS) structures. J Mater Sci Mater Electron 28:1315–1321. https://doi.org/10.1007/s10854-016-5662-3
22. Demirezen S (2013) Frequency- and voltage-dependent dielectric properties and electrical conductivity of au/PVA (bi-doped)/n-Si Schottky barrier diodes at room temperature. Appl Phys A Mater Sci Process 112:827–833. https://doi.org/10.1007/s00339-013-7605-7
23. Aydın ME, Türüt A (2007) The electrical characteristics of Sn/methyl-red/p-type Si/Al contacts. Microelectron Eng 84:2875–2882. https://doi.org/10.1016/j.mee.2007.02.010
24. Lapa HE, Kökce A, Özdemir AF, Altındal Ş Investigation of Dielectric Properties, Electric Modulus and Conductivity of the Au/Zn-Doped PVA/n-4H-SiC (MPS) Structure Using Impedance Spectroscopy Method. Z Phys Chem 234:505–516. https://doi.org/10.1515/zpch-2017-1091
25. Cowley AM, Sze SM (1965) Surface states and barrier height of metal-semiconductor systems. J Appl Phys 36:3212–3220. https://doi.org/10.1063/1.1702952

26. Altındal Ş, Kanbur H, Yıldız DE, Parlak M (2007) Current conduction mechanism in Al/p-Si Schottky barrier diodes with native insulator layer at low temperatures. Appl Surf Sci 253:5056–5061. https://doi.org/10.1016/j.apsusc.2006.11.015
27. Kang WP, Davidson JL, Gurbuz Y, Kerns DV (1995) Temperature dependence and effect of series resistance on the electrical characteristics of a polycrystalline diamond metal-insulator- semiconductor diode. J Appl Phys 78:1101–1107. https://doi.org/10.1063/1.360343
28. Ashery A, Elnasharty MMM, Hameed TA (2020) Investigation of electrical and dielectric properties of epitaxially grown au/n-GaAs/p-Si/Al heterojunction. Opt Quant Electron 52:490. https://doi.org/10.1007/s11082-020-02601-4
29. Ashery A, Farag AAM, Moussa MA, Turky GM (2021) Electrical performance of nanocrystalline graphene oxide/SiO2-based hybrid heterojunction device. Mater Sci Semicond Process 121:105415. https://doi.org/10.1016/j.mssp.2020.105415
30. Pakma O, Serin N, Serin T, Altındal Ş (2008) The double Gaussian distribution of barrier heights in Al/TiO2/p-Si (metal-insulator-semiconductor) structures at low temperatures. J Appl Phys 104: 14501. https://doi.org/10.1063/1.2952028
31. Mahani R, Ashery A, Elnasharty MMM (2019) Frequency and voltage dependence of the dielectric properties of Ni/SiO2/P-Si (MOS) structure. Silicon 12:1879–1885. https://doi.org/10.1007/s12633-019-00277-4
32. Cheung SK, Cheung NW (1986) Extraction of Schottky diode parameters from forward current-voltage characteristics. Appl Phys Lett 49:85–87. https://doi.org/10.1063/1.97359
33. Ashery A, Elnasharty MMM, Khalil AAI, Azab AA (2020) Negative resistance, capacitance in Mn/SiO2/p-Si MOS structure. Mater Res Express 7:85901. https://doi.org/10.1088/2053-1591/aba818
34. Buyukbas-Ulusan A, Tataroglu A (2020) Electrical characterization of silicon nitride interlayer-based MIS diode. J Mater Sci Mater Electron 31:9888–9893. https://doi.org/10.1007/s10854-020-03533-1
35. Norde H (1979) A modified forward I-V plot for Schottky diodes with high series resistance. J Appl Phys 50:5052–5053. https://doi.org/10.1063/1.325607
36. Tatarŏlu A, Hendi AA, Alorainy RH, Yakuphanŏlu F (2014) A new aluminum iron oxide Schottky photodiode designed via sol—gel coating method. Chinese Phys B 23:57504. https://doi.org/10.1088/1674-1056/23/5/057504
37. Chaudhry MA, Jonscher AK (1988) High-temperature dielectric properties of ruby mica perpendicular to the cleavage planes. J Mater Sci 23:208–216. https://doi.org/10.1007/BF01174055
38. Fleig J, Maier J (2004) The polarization of mixed conducting SOFC cathodes: effects of surface reaction coefficient, ionic conductivity and geometry. J Eur Ceram Soc 24:1343–1347. https://doi.org/10.1016/S0955-2219(03)00561-2
39. Smari M, Rahmouni H, Elghoul N, Walha I, Dhahri E, Khirouni K (2015) Electric–dielectric properties and complex impedance analysis of La0.5Ca0.5−xAgxMnO3 manganites. RSC Adv 5:2177–2184. https://doi.org/10.1039/C4RA11323C
40. Suman CK, Prasad K, Choudhary RNP (2006) Complex impedance studies on tungsten-bronze electroceramic: Pb2Bi3LaTi5O18. J Mater Sci 41:369–375. https://doi.org/10.1007/s10853-005-2620-5
41. Prasad K, Kumar A, Choudhary SN, Choudhary RNP (2005) Relaxor behaviour of Pb[(Mg3/4Co1/4)1/3Nb2/3]O3 ceramic. Solid State Ionics 176:1641–1646. https://doi.org/10.1016/j.ssi.2005.04.004
42. Büyükbaş-Uluşan A, Tataroğlu A (2020) Impedance spectroscopy of au/TiO2/n-Si metal-insulator-semiconductor (MIS) capacitor. Phys B Condens Matter 580:411945. https://doi.org/10.1016/j.physb.2019.411945
43. Rao KS, Murali Krishna P, Madhava Prasad D, Lee JH, Kim JS (2008) Electrical, electromechanical and structural studies of lead potassium samarium niobate ceramics. J Alloys Compd 464:497–507. https://doi.org/10.1016/j.jallcom.2007.10.023
44. Ashery A, Farag AAM, Moussa MA, Turky GM (2020) Enhancement of electrical and dielectrically performance of graphene-based promise electronic devices. Synth Met 261: 116303. https://doi.org/10.1016/j.synthmet.2020.116303
45. Ashery A, Elnasharty MMM, El Radaf IM (2020) Current transport and dielectric analysis of Ni/SiO2/P-Si diode prepared by liquid phase Epitaxy. Silicon. https://doi.org/10.1007/s12633-020-00808-4
46. Ashery A, Shaban H, Gad SA, Mansour BA (2020) Investigation of electrical and capacitance- voltage characteristics of GO/TiO2/n-Si MOS device. Mater Sci Semicond Process 114:105070. https://doi.org/10.1016/j.mssp.2020.105070
47. Ashery A, Gad SA, Shaban H (2020) Frequency and temperature dependence of dielectric properties and capacitance–voltage in GO/TiO2/n-Si MOS device. Appl Phys A Mater Sci Process 126:547. https://doi.org/10.1007/s00339-020-03729-6
48. Ashery A, Moussa MA, Turky GM (2021) Enhancement of electrical and dielectric properties of Graphene oxide-nanoparticle based devices. Silicon. https://doi.org/10.1007/s12633-021-00943-6